ISSN 0869-5911, Petrology, 2020, Vol. 28, No. 4, pp. 389–401. © Pleiades Publishing, Ltd., 2020.
Russian Text © The Author(s), 2020, published in Petrologiya, 2020, Vol. 28, No. 4, pp. 431–445.

Small-Scale Reactional Features in Abyssal Peridotites from the Mid-Atlantic Ridge at 17°04′ to 17°10′ N

A. N. Pertsev[a], * and V. E. Beltenev[b]

[a] *Institute of Geology of Ore Deposits, Petrography, Mineralogy, and Geochemistry, Russian Academy of Sciences, Moscow, Russia*

[b] *Stock Venture "Polar marine geosurvey expedition", St.-Petersburg–Lomonosov, Russia*

**e-mail: alexei_n@igem.ru*

Received December 9, 2018; revised December 24, 2019; accepted December 29, 2019

Abstract—Serpentinized peridotites (lherzolite to harzburgite) with relict coarse-grained protogranular and porphyroclastic matrix and locally developed fine-grained spinel–pyroxene microstructures were sampled from a previously unknown tectonic exposure of the Mid-Atlantic Ridge (17°04′–17°10′ N). The mineral composition of the coarse-grained relics is typical of abyssal residual peridotites and corresponds to 13–14% fractional melting. Fine-grained spinel-pyroxene (spinel–orthopyroxene and spinel–two-pyroxene) intergrowths are regarded as traces left by peridotite interaction with an interstitial melt during the transition to the lithospheric conductive cooling at temperature of 1100–1000°C. The peridotite–melt interaction resulted in the partial orthopyroxene dissolution, local crystallization of spinel ± clinopyroxene, and uneven decrease of Al and Cr contents in both pyroxenes and Cr/Al ratio in spinel. An additional signature of the reaction melt is an overall trend of enrichment in magmatic components: clinopyroxene in REE and spinel in Zn. The inferred interstitial reaction melt was significantly depleted in incompatible elements compared to MORB-type melts. Further lithospheric cooling favored "freezing" of mineral assemblages and small-scale reactional features.

Keywords: abyssal peridotite, reactional features, interstitial melt, spinel, pyroxene, REE, lithosphere, conductive cooling

DOI: 10.1134/S0869591120040062

INTRODUCTION

According to the modern concepts, abyssal (oceanic) peridotites and their ophiolite analogues are of primary residual nature, i.e. are refractory residue left after extraction of basaltic melts under spreading centers through variable degree of adiabatic decompressional mantle melting (e.g., Dick et al., 1984; Johnson et al., 1990; Walter, 2003). Further structural-compositional transformations of the residual rocks are accompanied by interaction with mantle melts coming from different depths depending on structural-geodynamic settings. The interaction may occur with intergranular melt films and with focussed flows in high-permeability channels by the diffusion crystal/melt exchange as well as by dissolution and crystallization of minerals with significant change of not only geochemical but also modal composition (e.g., Kelemen et al., 1994; Niu et al., 1997; Reiners, 1998; Asimow, 1999; Godard et al., 2000; Seyler et al., 2003; Rampone et al., 2004).

MORB-type melts entering the upper lithospheric horizons beneath volcanic spreading centers are saturated in olivine and undersaturated in both pyroxenes (Kelemen et al., 1994). The correlation of whole-rock and modal composition confirms the crystallization of olivine and dissolution of pyroxenes with decreasing modal clinopyroxene/orthopyroxene ratio (Asimow, 1999; Rampone et al., 2004). Similar process could occur in a system of highly-permeable channels represented by a network of dunite veins in the upper mantle peridotites and/or in the dunitic mantle–crustal transition zone in ophiolites, where the local dunite/MORB equilibrium is likely reached at high melt/rock ratio (Kelemen et al., 1994; Suhr, 1999; Godard et al., 2000). Of great importance also is sublithospheric peridotite–melt interaction with opposite trends ("refertilization"), i.e., a change of bulk composition from harzburgite to lherzolite and enrichment in incompatible elements. Corresponding melts may come from different magma generation levels and differ in composition from MORB (e.g., Brunelli et al., 2006, 2014). Mineralogical and microstructural features of refertilization are preserved much worse due to the solid-state ductile flow of peridotite matrix in high-temperature asthenospheric conditions. Nevertheless, some microstructural heterogeneities in peridotites in form of late clinopyroxene generations, par-

tial replacement of orthopyroxene by clinopyroxene and/or by spinel–clinopyroxene microaggregate are interpreted as traces of incomplete extraction of interstitial melts during the transition to the lithospheric conductive cooling conditions and described in the slow to ultraslow spreading associations of abyssal peridotites and ophiolites (Seyler et al., 2001, 2007; Suhr et al., 2008; D'Errico et al., 2016; Wang et al., 2019). The preservation of such microstructural heterogeneities is explained by "freezing" of solid–state ductile flow in a thick cold lithosphere beneath the slow- and ultraslow-spreading centers (Suhr et al., 2008).

The microstructural heterogeneities in abyssal peridotites are difficult to identify due to their poor preservation under high-temperature conditions and further alteration in the tectonic exposures of high-Mg rocks on the ocean floor. Due to significant hydrothermal alterations and submarine weathering of most tectonic exposures of abyssal peridotites, it is impossible not only to observe the microstructural features, but even to find relics of mantle silicate minerals. This work reports new data on the previously unknown exposure of abyssal peridotites in geological environment of tectonic extension of the Mid-Atlantic ridge. The studied samples were collected during 37th cruise of the R/V *Professor Logachev*. In particular, during this cruise we recognized and sampled for the first time several exposures of serpentinized ultramafics in the flanks of the MAR rift valley at 16°43′–17°32′ N. Of most interest among these exposures is peridotite massif, which is intruded by gabbroic rocks and cropped out in the eastern flank of the rift valley at 17°04′–17°10′ N. In this massif, unlike adjacent massifs, serpentinized rocks locally retained relics of mantle minerals and reactional microstructures. The main attention is focused on the structural–compositional heterogeneity of minerals. We attempted to reconstruct the chemical trends during formation of local reactional structures on the basis of representative analytical data.

METHODS

Dredge and TV-grab sampling during cruise made it possible to distinguish an extensional structure with gabbro-peridotite core and to collect rock samples for laboratory studies, which involved a complex study of polished thin sections: petrographic description, recognition of local mineral assemblages, and microprobe analysis.

Major-element composition of minerals and BSE images were performed using a JEOL Superprobe 8200 at the Center for Collective Use "IGEM-ANALITIKA" by S.E. Borisovskiy (Moscow). Operating conditions: accelerating voltage of 20 kV, beam current of 50 nA, and focused beam spot diameter 1 to 5 μm depending on required conditions. Correction for the average atomic number, absorption, and secondary fluorescence was introduced using the ZAF-correction. Natural minerals were used as standards for calibration.

Trace element abundances in clinopyroxene were determined using the secondary-ion mass spectrometry (Shimizu and Hart, 1982) on a CAMECA IMS 4f ion microprobe at the Yaroslavl Branch of the Institute of Physics and Technology, Russian Academy of Sciences (YaF FTIAN), analysts S.G. Simakin and E.V. Potapov. A primary beam of O_2^- ion accelerated to 10 keV (14.5 keV at the sample surface) was focused on the sample over a spot diameter about 30 μm, at a primary ion current of 5–8 nA. The intensity of positive secondary ions ^{30}Si, ^{89}Y, ^{154}Gd, ^{156}Gd, ^{158}Gd, ^{162}Dy, ^{163}Dy, ^{167}Er, ^{174}Yb was determined using a sample offset voltage of 100 V and energy window of 50 eV (Sobolev, 1996). Each measurement included five cycles of signal accumulation, the duration of which depended on the intensity. The secondary ion intensities were calculated relative to ^{30}Si and abundances were calculated using Si concentration obtained by electron microprobe analysis. Corrections for overlapping REE oxides on the Gd, Yb, and Er values were calculated according to (Botazzi et al., 1994). Augite KH-1 (Irving, Frey, 1984) was used for calibration.

GEOLOGICAL POSITION AND SAMPLING

The described exposure of deep-seated rocks is located in the Mid-Atlantic Ridge (MAR) segment between the Fifteen Twenty fracture zone (15°20′ N) in the south and the Vidal fracture zone (17°50′ N) in the north. Data obtained during 37th Cruise of the R/V *Profesor Logachev* show that the rift valley of MAR at 17°03′–17°10′ N has a sharply asymmetric morphology (Fig. 1a). The eastern flank rises 2.5 km above the rift valley floor. According to bathymetric studies, the least fixed depth of the eastern flank summit is less than 1500 mbsl (meters below sea level), which is an absolute regional minimum. The western flank rises up to 500 m above the valley floor and is complicated by a spacious terrace 3–6 km wide. The valley floor is located at a water depth of 3500–4000 mbsl, deepening southward down to 4500 mbsl. The floor is 6–10 km wide. The neovolcanic rise (NVR) with well preserved and sampled basaltic lavas joins the eastern margin of the floor.

More detailed study of the eastern flank of the rift valley was carried out in relation with the discovery in 2015 of two sulfide–base metal "black smoker" vent fields developed on serpentinites (Pobeda-1 and -2, Fig. 1a). According to the results of mapping sampling at 27 stations, the serpentinized rocks with subordinate gabbroids are exposed in the eastern flank of the valley, above depths of 4500–3000 mbsl (Fig. 1b). Upslope to the east, the gabbro–peridotite association at depths less than 2000–2500 mbsl grades into basalts with poorly preserved chilled zones of pillow lavas. Samples of the serpentinized peridotites were col-

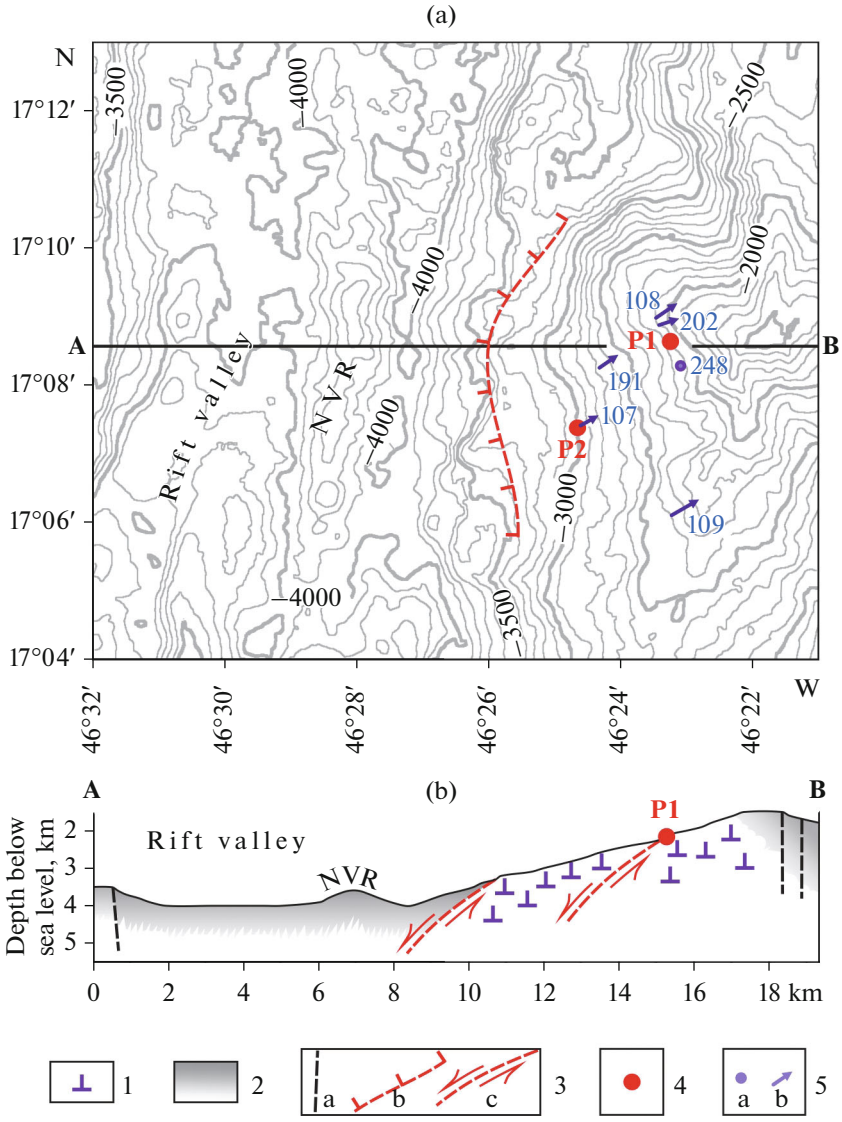

Fig. 1. Bathymetric map (a) and cross-section A–B (b) with interpretation of the geological structure of MAR at 17°04′–17°13′ N. (1) rocks of the gabbro–ultramafic association; (2) basalts; (3) inferred faults ((a) subvertical low-offset faults in cross-section, (b, c) low-angle large-offset extensional fault in the map and cross-section, respectively); (4) Pobeda-1 and -2 hydrothermal fields (P1 and P2, respectively); (5) peridotite sampling localities collected with (a) TV-grab and (b) dredge (Table 1). Other 21 stations are not shown. NVR is the neovolcanic rise (magmatic center of spreading). In section, the vertical scale equals horizontal one.

lected from 17 stations at 17°04′–17°10′ N. The interpretation of the asymmetric geological structure (Fig. 1b) is based on the concepts of slow-spreading extensional structures typical of MAR, where footwalls of low-angle large-offset extensional faults expose mantle peridotite cores intruded by gabbroic rocks without developing of volcanic cover (Karson and Lawrence, 1997; MacLeod et al., 2009; Smith et al., 2008). The presence of low-angle large-offset extensional fault (Fig. 1b) is confirmed by active sulfide hydrothermal fields ("black smokers"), which develop on periodites well away from the rift valley axial zone (McCaig et al., 2007; Petersen et al., 2009).

PETROGRAPHY

A collection of variably altered spinel peridotites was sampled in the eastern flank of the MAR rift valley at 17°04′–17°10′ N (Fig. 1a). In addition, unevenly distributed plagioclase and gabbroic veinlets were identified in two peridotite samples. Nine samples taken for complex study from six stations (Table 1, Fig. 1a) locally retained relict peridotite textures and mineral assemblages with no signs of interaction with gabbroids. Most samples with preserved relics of primary minerals retained primary medium- to coarse-grained protogranular, locally transitional to the porphyro-

Table 1. Technical characteristics of sampling stations with numbers of studied samples

Station number	Device of sampling	Latitude (northern), degree	Longitude (eastern), degree	Depth, m	Sample no.
37L107	Dredge	17.1237	46.4105	3003	107-12,
		17.1256	46.4071	2790	107-19
37L108	Dredge	17.1497	46.3913	2105	108-01,
		17.1533	46.3859	1968	108-10
37L109	Dredge	17.1017	46.3873	2400	109-05
		17.1056	46.3804	2190	
37L191	Dredge	17.1381	46.4047	2658	191-06
		17.1404	46.4013	2550	
37L202	Dredge	17.1483	46.3894	2033	202-01
		17.1493	46.3861	1950	
37L248	TV-grab	17.1381	46.3851	2115	248-06,
					248-07

clastic texture (Suppl. 1[1], Figs. ESM_1.pdf, ESM_2.pdf). In addition, these samples are characterized by locally overprinted spinel–pyroxene microaggregates (Figs. ESM_2.pdf, ESM_3.pdf).

Medium to Coarse-Grained Aggregates

Relict peridotite aggregate (Fig. ESM_1.pdf, A) consists of olivine (Figs. ESM_1.pdf A, B), orthopyroxene (Figs. ESM_1.pdf, A, C), clinopyroxene (Fig. ESM_1.pdf, A, C, D), and spinel (Fig. ESM_1.pdf, E, F) at uneven distribution of the two latters. The average modal content of olivine is approximately 70–80%. According to the classification, the mineral composition of primary peridotites is close to the lherzolite–harzburgite transition, i.e., the average content of clinopyroxene is about 5%. The spinel content is less than 1%.

Olivine forms grains with primary size up to 5 mm, as judged from relics with simultaneous extinction within cells of reticulate serpentinization texture (Figs. ESM_1.pdf, A, B and ESM_2.pdf, A). Locally, olivine retains intracrystalline deformations represented by kink bands.

Orthopyroxene occurs as grains up to 5–8 mm size and in the intergrowths with clinopyroxene (Fig. ESM_1.pdf, A). The grains are often deformed, which is expressed as bent cleavage. Sometimes, 0.1–1 mm neoblasts of ortho- and clinopyroxene are observed around orthopyroxene porphyroclasts up to few mm size (Fig. ESM_1.pdf, C). Orthopyroxene contains submicron clinopyroxene exsolution lamellae.

Clinopyroxene is represented by deformed, frequently porphyroclastic grains up to 10 mm in size, as well as intergrowths with orthopyroxene grains (Fig. ESM_1.pdf, A, D). The mineral contains submicron orthopyroxene lamellae. A minor amount of clinopyroxene form neoblasts 0.1–1 mm in size (Fig. ESM_1.pdf, C).

Spinel is observed as translucent, red-brown, typically anhedral grains up to 2–5 mm in size in the interstices between large silicate grains, frequently with branching offshoots (Fig. ESM_1.pdf, E, ESM_2.pdf, B). Sometimes spinel contains olivine inclusions up to 0.2 mm in size. Euhedral spinel is less common (Fig. ESM_1.pdf, F).

Spinel–Pyroxene Microaggregates

Superimposed spinel–pyroxene microaggregates are characteristic feature of the studied peridotites, although they are unevenly distributed and occupy an insignificant volume. These microaggregates are observable optically (Figs. ESM_2.pdf, C; ESM_3.pdf, A, B), but the correct pyroxene identification is more preferable by scanning electron microscopy (Figs. ESM_3.pdf, C, D). The microaggreagtes develop in the rims of large orthopyroxene, frequently along the contact with olivine. Orthopyroxene in the microaggregate preserves optical orientation of large host mineral. Such aggregates often show symplectite appearance, with fine vermiform spinel patterns amounting ca. 20–25 vol % (Figs. ESM_3.pdf, C, D). Proportions of ortho- and clinopyroxene show wide variations. Some aggregates have clinopyroxene-free spinel–orthopyroxene composition (Figs. ESM_3.

[1] The textural features of the studied peridotites are shown in Figs. ESM_1.pdf–ESM_3.pdf (Suppl. 1) to the Russian and English on-line version on sites https://elibrary.ru/ and http://link.springer.com/, respectively.

pdf, A, C), whereas others are dominated by clinopyroxene (Fig. ESM_2.pdf, C; ESM_3.pdf, D) or have intermediate proportions of both pyroxenes (Fig. ESM_3.pdf, B). Unlike medium to coarse-grained peridotite aggregate, pyroxene in spinel–pyroxene microaggregates is typically free of exsolution lamellae. Olivine is not visible in the spinel-pyroxene microaggregates. Pictures in Fig. ESM_3.pdf show that the local mineral assemblages of the spinel-pyroxene aggregates are generally well distinguishable from those in the coarser grained peridotite textures.

Similar overprinting of spinel–pyroxene microstructures have been previously described in the abyssal harzburgites from hole 1274 ODP in the same MAR segment (15°39′ N) (Seyler et al., 2007; Suhr et al., 2008), together with other types of superimposed symplectite microstructures, which are absent in our samples. Such microstructures are interpreted as traces of the interaction between orthopyroxene and intergranular melt with decreasing *P-T* parameters: dissolution of orthopyroxene with depletion of its rest part in $Mg(Al, Cr)AlSiO_6$ and $CaSiO_3$; redistribution of Al_2O_3 and Cr_2O_3 from orthopyroxene and the melt into crystallizing spinel, and SiO_2 and CaO into the melt; crystallization of clinopyroxene at sufficient accumulation of CaO and SiO_2 in the melt (Seyler et al., 2007). Similar pyroxene–spinel symplectite microstructures were also noted in the abyssal peridotites from the ultraslow-spreading settings: in lherzolite from the Gakkel Ridge (D'Errico et al., 2016) and harzburgites from the Southwest Indian Ridge (Wang et al., 2019).

Secondary Alterations

Multistage hydrothermal alterations are expressed in the replacement of clinopyroxene by hornblende with removal of Ca, subsequent overall serpentinization of olivine accompanied by escape of Mg, talcization and bastitization of orthopyroxene, and partial replacement of spinel by magnetite. The later processes include chloritization, development of chrysotile microveinlets, and carbonatization. The carbonatization occurs as the wide development of calcite pseudomorphs after olivine relics in cells of reticulate serpentinization texture, as well as aragonite veinlets enriched in Sr. Occasional cross-cutting veinlets of native copper are likely related to the highest temperature hydrothermal events, whereas iron sulfides record the lower temperature events. The secondary processes in general strongly affect the proportions of rock-forming elements (Si, Fe, Mg, Ca). Therefore, the whole-rock compositions do not seem informative for studying the superimposed microstructures. The main attention in our work is focused on the detailed study of mineral composition.

MINERAL COMPOSITION

To find regularities in the compositional heterogeneity of minerals, we divide pyroxenes and spinels into three assemblages based on their petrographic features: (1) cores of large (>1 mm) grains in the medium to coarse-grained aggregates; (2) rims of large grains and tiny grains, including neoblasts and spinel interstitial offshoots in the medium to coarse-grained aggregates; (3) superimposed spinel–pyroxene microaggregates. These three assemblages are well distinguishable for orthopyroxene, clinopyroxene, and spinel. The mineral varieties are, respectively, abbreviated as $Opx_{1, 2, 3}$, $Cpx_{1, 2, 3}$, and $Spl_{1, 2, 3}$. Olivine cannot be assigned to assemblages (1) and (2) due to its fragmentary preservation and is absent in (3). Analyses of pyroxenes and spinel are presented in Suppl. 2[2]: tables ESM_4.xls–ESM_7.xls.

The **olivine** composition is typical of abyssal peridotites. It shows no systematic variations within one sample or the entire studied collection: average forsterite content is 90.34 ± 0.31 mol. %. The admixtures of MnO, NiO, and CaO are 0.130 ± 0.025, 0.39 ± 0.03, and 0.046 ± 0.018 wt %, respectively.

Orthopyroxene. In terms of Mg# ($100 \times Mg/(Mg + Fe)$, atomic ratio) and TiO_2 admixture, Opx_1, Opx_2, and Opx_3 have no general differences. Mg# on average accounts for 90.93 ± 0.38, TiO_2 content is < 0.15 wt %, averaging 0.04 ± 0.02 wt %. (ESM_4.xls).

Orthopyroxene shows significant variations in Cr/Al ratios regardless of the distinguished varieties (Fig. 2). It is suggested that the orthopyroxenes in abyssal peridotites display general depletion in Al_2O_3 and enrichment in Cr_2O_3 with increasing degree of partial melting due to opposite compatibility of Al and Cr with a melt and crystalline aggregate (e.g., Seyler et al., 2003; Brunelli et al., 2003). The negative correlation between Cr and Al related to depletion is markedly complicated by trends of decreasing $Mg(Al,Cr)AlSiO_6$ solubility in orthopyroxene with decreasing *P-T* conditions during asthenosphere–lithosphere transition (Seyler et al., 2003, 2007). Since the effect of the overlapping trends on the decrease in Cr# ($100 \times Cr/(Cr + Al)$, atomic ratio) is less pronounced, the studied orthopyroxenes may be shown against the general trend of abyssal peridotite depletion in the Al_2O_3 versus Cr# plot (Fig. 2a). In Fig. 2a, the degree of depletion of peridotites at 17°04′–17°10′ N MAR is slightly higher than the mean values of abyssal peridotites from slow- to ultraslow spreading ridges.

Regardless of the distinguished varieties ($Opx_{1,2,3}$) orthopyroxenes show a common trend of simultaneous decrease in Al and Cr contents (Fig. 2b), which

[2] Chemical compositions of minerals and studied peridotites are shown in Tables ESM_4.xls—ESM_7.xls (Suppl. 2) to the Russian and English online versions on sites https://elibrary.ru/ and http://link.springer.com/, respectively.

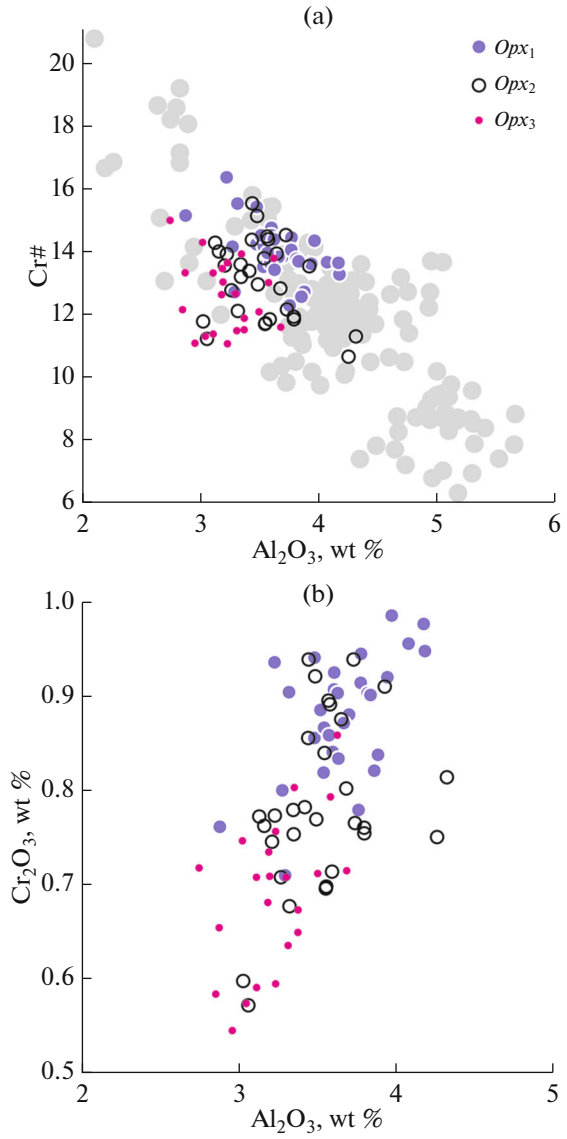

Fig. 2. Al–Cr variations in orthopyroxene. Gray color shows the orthopyroxene compositions in the abyssal peridotites from slow and ultraslow spreading ridges according to (Michael and Bonatti, 1985; Dick, 1989; Komor et al., 1990; Ghose et al., 1996; Stephens et al., 1997; Brunelli et al., 2003).

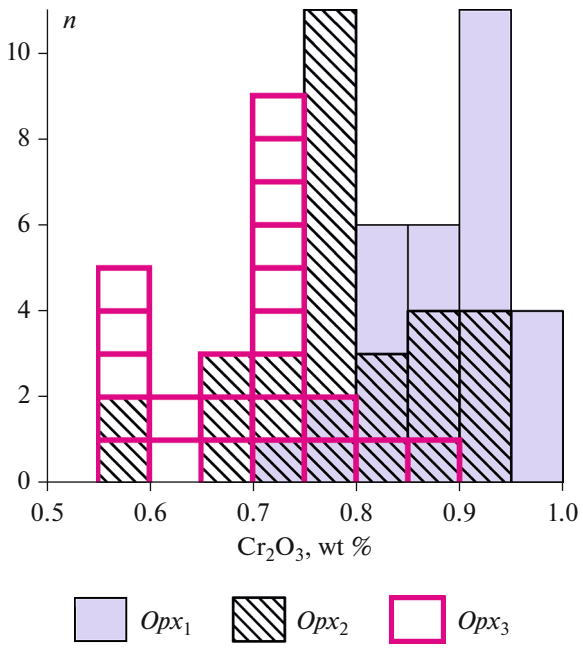

Fig. 3. Distribution of Cr_2O_3 contents over three distinguished petrographic orthopyroxene varieties. Vertical axis is number of analyses (*n*) (Suppl. 2, ESM_4.xls).

corresponds to the gradual purification of $Opx_{2,3}$ from Cr and Al admixtures compared to Opx_1. This general trend is complicated by a significant compositional overlap. In particular, approximately half of the cores of large grains are also relatively depleted in Cr and Al. Nevertheless, the statistical maxima of Cr_2O_3 variations in Opx_1, Opx_2, and Opx_3 are more or less separated (Fig. 3).

Clinopyroxene. Mg# in clinopyroxene is within 90.3–93.5, showing no systematic variations. The Al–Cr relations are the same as in orthopyroxene. Like orthopyroxenes, the studied clinopyroxenes correspond to a slightly higher degree of depletion than the average for abyssal peridotites (Fig. 4a). Unlike orthopyroxenes, the varieties $Cpx_{1,\,2,\,3}$ are better distinguished in the Al_2O_3–Cr_2O_3 diagram (Fig. 4b). TiO_2 contents of $Cpx_{1,\,2,\,3}$ significantly overlap, although a general trend of increasing TiO_2 with Cr# decrease is visible (Fig. 4c).

The LREE and MREE contents are less than a hundredth of one ppm in the studied clinopyroxene, which is below detection limit of secondary ion mass spectrometry. Quantitative data were obtained only for HREE (Gd, Dy, Er and Yb), and Y. We carried out 15 local analyses of Cpx_1, one analysis of Cpx_2, and five analyses of Cpx_3 (Table ESM_7.xls). The spectra of Ti, Gd, Dy, Y, Er, and Yb arranged in order of decreasing incompatibility of the elements (Sun and McDonough, 1989) reveal a significant heterogeneity of Cpx_1 with separation of the most Ti depleted compositions (Fig. 5a). Other 12 Cpx_1 analyses define a range of relatively enriched compositions with the higher enrichment in more incompatible Ti, Gd, and Dy than in less incompatible Y, Er, and Yb. Available Cpx_2, and Cpx_3 compositions correspond to the upper part of Cpx_1 range (Fig. 5a). Dy and Dy/Yb ratio can thus serve as indicators of relative enrichment and display a general trend (Fig. 5b). According to Dy and Dy/Yb values the most depleted composition is preserved only in three lowest Ti cores of large clinopyroxene grains, which fall in the shaded field in Fig. 4c. Significant part of Cpx_1 experienced enrichment likely

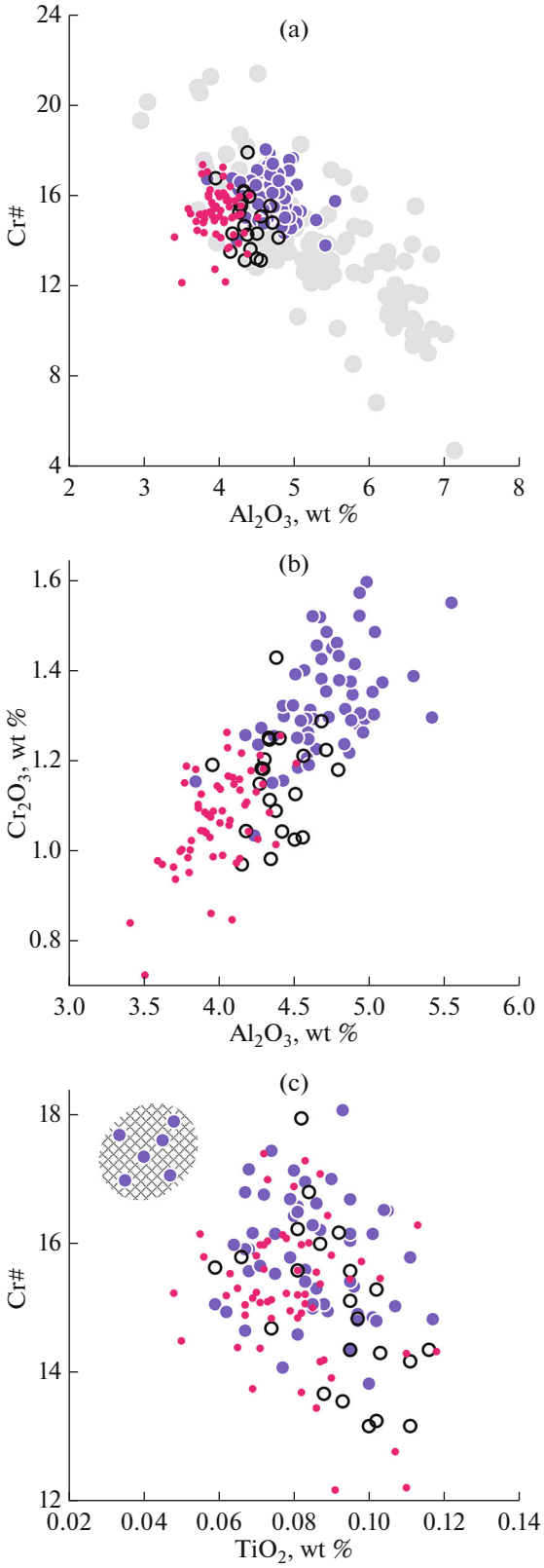

Fig. 4. Clinopyroxene compositional variations. Symbols are analogous to those for orthopyroxene in Fig. 1. Shaded field in the diagram (c) shows the composition of the earliest clinopyroxene.

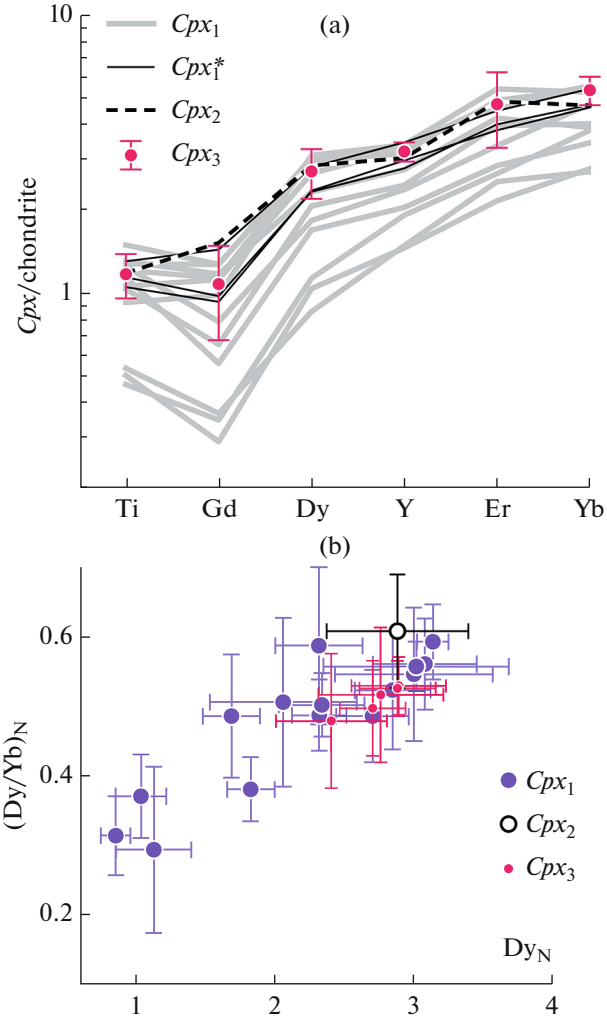

Fig. 5. Variations of trace incompatible elements in clinopyroxene: (a) trace-element spectra. Cpx_1^* are compositions used in further calculations; Cpx_3 – average of five local analyses with standard deviation ranges (1σ); (b) variations of Dy/Yb versus Dy with standard deviation ranges (1σ). Element concentrations are normalized to chondrite C1 (Sun and McDonough, 1989).

owing to the development of later spinel–pyroxene aggregates.

The study of clinopyroxene geochemistry in the abyssal peridotites with spinel–pyroxene microaggregates at 15°39' N MAR revealed its homogenous composition with no differences in REE spectra between clinopyroxene structural varieties, which is explained by the clinopyroxene equilibration with interstitial melt (Seyler et al., 2007).

Spinel. Cr# of spinel from spinel peridotites is one of the main indicators of the degree of mantle depletion (Hellebrand et al., 2001, 2002). In terms of Cr# and forsterite content in associated olivine, Spl_1 corresponds to a relatively depleted portion of the range

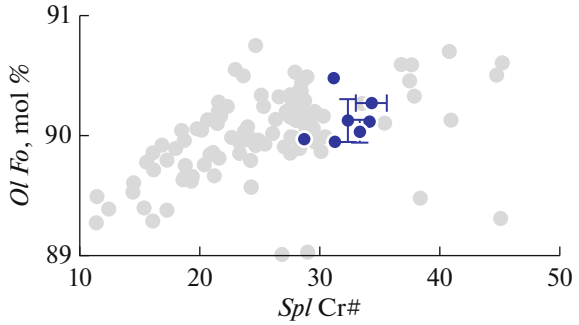

Fig. 6. Diagram spinel Cr# versus Fo content in associated olivine. Standard deviation ranges (1σ) are shown if they exceed symbol size. The gray color shows associations of abyssal peridotites from the slow and ultraslow spreading settings according to (Michael and Bonatti, 1985; Dick, 1989; Komor et al., 1990; Ghose et al., 1996; Stephens et al., 1997; Brunelli et al., 2003).

typical of abyssal peridotites from slow- and ultraslow spreading ridges (Fig. 6).

The differences between Spl_1, Spl_2, and Spl_3 are visible in Cr# and Mg# values (Fig. 7a). A transition from Spl_1 to $Spl_{2,3}$ is generally accompanied by a simultaneous decrease in Mg# and Cr#. This correlation can be explained by retrograde re-equilibration with pyroxenes and interstitial melt owing to the limited solubility of $Mg(Al,Cr)AlSiO_6$ in pyroxenes and silicate–spinel reactions of Mg-Fe exchange. At the same time, Spl_2 and Spl_3 with the lowest Mg# and Cr# (most distant from the main field of Spl_1 compositions) in general reveal a negative correlation between Cr# and Mg#, which can be explained by further retrograde silicate/spinel re-equilibration without participation of melt and change of Cr#. This is caused by the higher chemical affinity of higher Cr# spinels to Fe^{2+} relative to Mg (Aranovich and Kosyakova, 1980; Aranovich, 1991). The compositions of Spl_1 with the highest Cr# and Mg# are clustered as a separate field, which includes one analysis of Spl_2 and none of Spl_3 (Fig. 7a). This field shown by shading in Fig. 7a likely most closely reflects the primary composition of residual spinel with Cr# 33.8–35.5. According to the empirical formula (Hellebrand et al., 2001), the corresponding degree of fractional melting is approximately 13–14% (Hellebrand et al., 2001). Another important peculiarity of the studied spinel is a general relative enrichment in ZnO from Spl_1 to $Spl_{2,3}$ (Fig. 7b).

DISCUSSION

Presented data on mineral composition show that the studied ultramafic rocks are ascribed to typical residual abyssal peridotites with locally preserved protogranular to porphyroclastic medium and coarse-grained textures. The composition of primary spinel in the medium and coarse-grained aggregates corresponds to ca. 13–14% partial fractional melting.

The presence of spinel–two pyroxene assemblage both in the medium-grained matrix and in spinel–pyroxene microaggregates of the studied spinel peri-

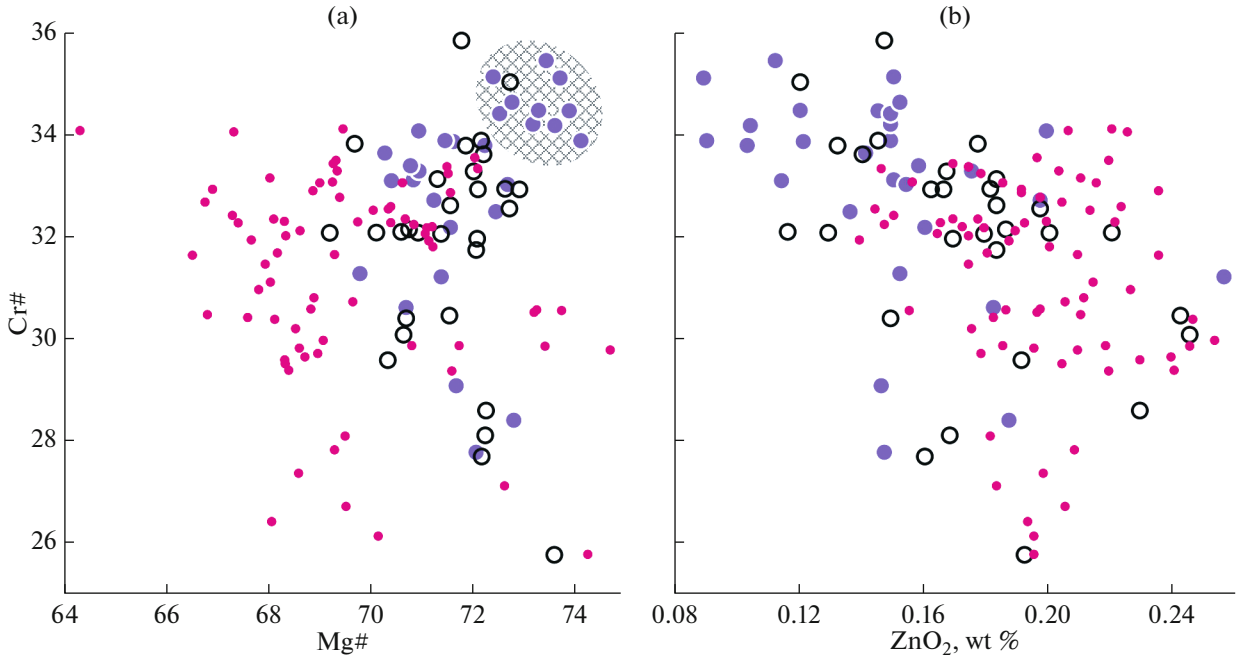

Fig. 7. Variations of spinel composition. Abbreviations Spl_1, Spl_2 , and Spl_3 are analogous to Opx_1, Opx_2 , and Opx_3 , respectively, in Fig. 2. Shaded field is the composition supposedly closest to the primary residual spinel.

dotites indicates their formation under spinel–peridotite facies conditions, i.e., at 1–2.2 GPa (O'Hara et al., 1971; Yoder, 1976; Gasparik, 2000), which approximately correspond to depths of 30–60 km and indicates the mantle ascent in the upper lithosphere horizons in a "frozen" state.

To evaluate temperature we used Al_2O_3 content in orthopyroxene in the assemblage with spinel and olivine, according to the model reaction:

$$\left[(Mg,Fe)_2 Si_2O_6\right]_{Opx} + \left[(Mg,Fe) Al_2O_4\right]_{Spl} = \left[(Mg,Fe) Al_2SiO_6\right]_{Opx} + \left[(Mg,Fe)_2 SiO_4\right]_{Ol}.$$

The Al_2O_3 solubility in orthopyroxene in this assemblage strongly depends on temperature and is practically pressure-independent (Kosyakova et al., 2005). This thermometer involves correction for Cr content in spinel (Kosyakova et al., 2005; Liermann and Ganguly, 2003) and has been already applied to abyssal peridotites (Pertsev et al., 2009). Unlike thermometers based on the Fe–Mg distribution, this method is characterized by the higher resolution and weak dependence on retrograde reactions of Fe–Mg exchange between coexisting minerals (Pattison and Begin, 1994; Aranovich and Berman, 1997).

In the high-Mg olivine–orthopyroxene assemblages, the Fe/Mg ratios of these coexisting minerals are very close ($XFa_{Ol} \approx XFs_{Opx}$), where XFa_{Ol} and XFs_{Opx} are the mole fractions of Fe_2SiO_4 in olivine and $FeSiO_3$ in orthopyroxene, respectively. While in moderate- and low-Mg assemblages $XFa_{Ol} > XFs_{Opx}$, a shift to the high-Mg region gradually provides inverse relations ($XFa_{Ol} < XFs_{Opx}$). According to experimental data, such inversion at Mg# ≈ 90 is expected at $T <$ 800°C (Aranovich and Berman, 1996). Since XFa_{Ol} and XFs_{Opx} in the studied samples vary from 0.083 to 0.095, the approximate equality ($XFa_{Ol} \approx XFs_{Opx}$) in local equilibria $Opx + Ol_{Opx}$ can apparently be shifted to one or another side. The best preservation is typical of the equilibrium assemblage $Spl_1 + Opx_1 + Ol$ in the early medium- and coarse-grained aggregates of spinel peridotites where in all cases $XFa_{Ol} > XFs_{Opx}$ with the highest temperature estimates. Equilibria of the same minerals in local assemblages of microaggregates reveal more complex compositional variations owing to retrograde processes. However, a predictable disequilibrium with only Mg–Fe redistribution between *Ol* and *Opx* during the low-temperature (400–750°C) transformations (Aranovich and Berman, 1996) very weakly affects the temperature estimates based on the Al solubility in orthopyroxene (Pattison and Begin, 1994; Aranovich and Berman, 1997). For example, the maximum range of XFa_{Ol} (0.084–0.094) in the studied peridotites was found in sample 37L108-10. Variations within this range correspond to error of ±15°C in calculated temperature.

Obtained temperature estimates (Table 2) for cores of the grains from medium- and coarse-grained aggregates ($Opx_1 + Spl_1 + Ol$) and rims of grains and neoblasts ($Opx_2 + Spl_2 + Ol$) are within 1150–1000°C and could be interpreted as a "freezing" temperature of solid-state ductile flow during transition from adiabatic asthenosphere conditions to lithospheric conductive cooling of peridotites (Suhr et al., 2008). Further cooling appears not to result in re-equilibration of $Opx_1 + Spl_1 + Ol$ and $Opx_2 + Spl_2 + Ol$ assemblages. It is suggested that such a transition with a change of physical state of mantle occurs at 1100–1000°C (Nicolas, 2012). Estimated temperatures for local $Opx_3 + Spl_3 + Ol$ assemblage in spinel–pyroxene microaggregates are within 1050–870°C. Temperatures below 1000°C for $Opx_3 + Spl_3$ likely reflect the late local recrystallization of some microaggregates at orthopyroxene grain boundaries and in the interstices under lithosphere conditions.

Compositional differences of pyroxenes and spinel in the cores of largest grains (Opx_1, Cpx_1, Spl_1) compared to their rims and neoblasts (Opx_2, Cpx_2, Spl_2), and spinel–pyroxene microaggregates (Opx_3, Cpx_3, Spl_3) are statistically visible with significant overlaps (Figs. 2, 3, 4, 7). We do not regard the studied spinel–pyroxene aggregates, including symplectites, as structures of garnet decompressional exsolution as proposed for some non-oceanic peridotite assemblages (e.g., Morishita and Arai, 2003; Falus et al., 2007; Odashima et al., 2008; Shimizu et al., 2008; Malaviarachchi et al., 2010; Obata and Ozava, 2011) for the clear reasons: (1) inconsistency with garnet composition, (2) absence of anomalous HREE enrichment of symplectite clinopyroxene (Cpx_3).

The shown clinopyroxene trend of enrichment in such magmatic components as Ti, REE, and Y (Figs. 4c, 5), and spinel enrichment in Zn (Fig. 7b) are consistent with concept that superimposed spinel–clinopyroxene microaggregates are traces of peridotite interaction with an interstitial melt at decreasing *P-T* conditions. Temperature estimates fit this concept, as they confirm "freezing" of mineral equilibria in the medium- and coarse-grained aggregates at temperatures typical of transition to the lithospheric conductive cooling (1150–1000°C).

Assuming that clinopyroxene most enriched in Ti, Gd, Dy, Y, Er, and Yb was in a local equilibrium with an interstitial melt, the temperature of these equilibria should be > 1000°C, because significant enrichment is observed also in the large grains of $Opx_1 + Spl_1$ structural assemblage (Fig. 5). We calculated possible concentrations of Gd, Dy, Y, Er, and Yb in reaction melt from equilibria with clinopyroxene using clinopyroxene/melt partition model for anhydrous melts (Wood and Blundy, 1997) and ionic radii from (Shannon, 1976). The calculations performed for Cpx_3 from the highest temperature local assemblage $Opx_3 + Spl_3 + Ol$

Table 2. Temperature estimated from orthopyroxene–spinel–olivine assemblage

Sample no.	Orthopyroxene: no. in ESM_4.xls	Spinel: no. in ESM_6.xls	Olivine *XFa*	Orthopyroxene *XFs*	*T*, °C
		$Opx_1 + Spl_1 + Ol$			
107-12	1	222–223	0.094	0.092	1070
107-19	2	225	0.095	0.089	1150
108-01	9	227	0.089	0.083	1070
108-10	12–15	238–241	0.093	0.086	1050
108-10	16–18	228–230	0.093	0.088	1110
191-06	21–23	242–244	0.093	0.086	1080
248-06	25	245–246	0.092	0.083	1080
248-07	30	250	0.094	0.090	1120
		$Opx_2 + Spl_2 + Ol$			
107-19	36	254–255	0.095	0.093	1060
191-06	46–47	260–262	0.093	0.088	1020
		$Opx_3 + Spl_3 + Ol$			
107-19	59	281	0.095	0.090	950
107-19	57	285	0.095	0.089	1020
108-01	61	287	0.086	0.083	930
109-05	62–65	298–303	0.088	0.085	910
109-05	66	304–305	0.086	0.081	870
202-01	68–70	327	0.094	0.090	1050
248-06	76–77	336–337	0.091	0.091	940

(1050°C, Table 2), as well as for three Cpx_1 compositions with the highest REE and Ti contents ("Cpx_1^*" in Fig. 5a). The given conditions are 1 GPa and 1100°C. Calculated concentrations of elements show an extremely depleted composition of melts compared to N-MORB in terms of absolute values and in spectra slopes (lower Gd/Yb and Dy/Yb ratios) (Fig. 8). Although using higher given temperature for clinopyroxene/melt equilibrium (e.g. 1200°C) should result in somewhat higher calculated concentrations of Gd, Dy, Y, Er, and Yb in the melt, the relations with N-MORB do not change considerably. Unlike peridotites studied at 15°39′ N MAR (Seyler et al., 2007), our assemblages reveal no superimposed LREE enrichment, which could be related to the more depleted geochemical type of the melt in our case. The preservation of microstructural traces of peridotite interaction with an interstitial melt could be explained by conditions of asthenosphere–lithosphere transitions, when a thick cold lithosphere in slow spreading settings provide rapid conductive cooling with "freezing" of mineral equilibria and microstructural heterogeneities (Suhr et al., 2008).

At the same time, some questions remain unanswered in the model of reaction interstitial melt (Seyler et al., 2007). The main question is the origin of melt that is reactive to orthopyroxene, but may crystallize clinopyroxene and spinel. According to Seyler et al. (with references to experimental works), such melt was likely an additional product of partial melting of lherzolites under spinel or garnet facies conditions (Seyler et al., 2001). If the reaction melt had a deeper-seated origin, in which proportions it mixed with shallower partial melts? It is also unclear what and to what degree influenced the local clinopyroxene and spinel enrichment in magmatic components: influx of interstitial melt or its partial crystallization at the beginning of cooling?

CONCLUSIONS

Serpentinized ultramafics at 17°04′–17°10′ N MAR exhumed in the footwall of the detachment fault have been studied for the first time. The ultramafics are ascribed to the abyssal spinel peridotites of lherzolite–harzburgite composition. The composition of primary chrome spinel corresponds to the 13–14% fractional depletion. The overprint of spinel–pyroxene microaggregates on the medium- to coarse-grained protogranular and porphyroclastic matrix could be explained by the reaction influence of an interstitial melt with partial dissolution of orthopyroxene and crystallization of late spinel and clinopyroxene. The process was accompanied by a general decrease of Al and Cr concentrations in pyroxenes, Ca

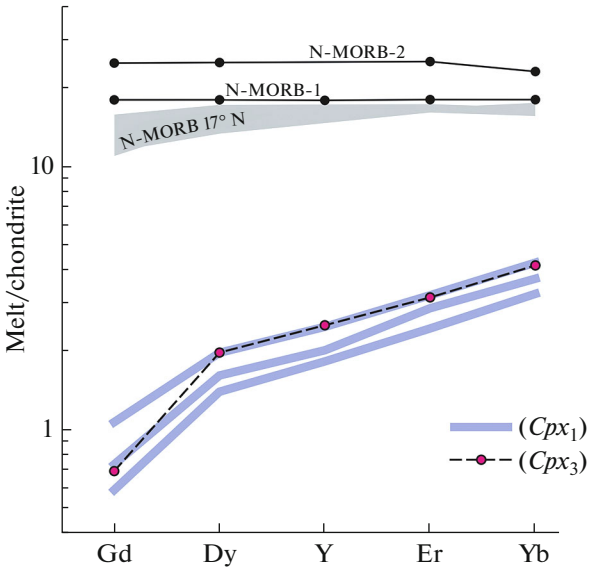

Fig. 8. Concentrations of Gd, Dy, Y, Er, and Yb in the reaction melt calculated from composition of enriched Cpx_1 and Cpx_3 from the highest temperature local assemblage $Opx_3 + Spl_3 + Ol$. Generalized compositions of N-MORB-1 and -2 are shown for comparison (Sun and McDonough, 1989; Hofmann, 1988, respectively). MORB 17° N is the bulk composition of basaltic lavas from NVR (Fig. 1) at 17°06'–17°10' N (V.E. Beltenev, unpublished data). Element concentrations are normalized to C1 chondrite (Sun and McDonough, 1989).

content in orthopyroxene, and Cr/Al ratio in spinel. The interstitial melt also caused an enrichment of minerals in magmatic components: clinopyroxene in Ti, REE, and Y and spinel in Zn. The interaction with the interstitial melt occurred under spinel facies conditions at temperatures above 1000°C and could be caused by a decrease of *P-T* conditions during transition to the lithosphere conductive cooling with subsequent "freezing" of mineral equilibria and structural microheterogeneities. The inferred interstitial melt was significantly depleted in incompatible elements compared to the MORB-type melts.

ACKNOWLEDGMENTS

We gratefully acknowledge L.Y. Aranovich for helpful discussions S.A. Silantyev, G.V. Ledneva, and anonymous reviewer are thanked for critical reviews of the first version of the manuscript.

FUNDING

This work was made in the framework of the State Task of IGEM RAS (project no. 0136-2018-0025) and was financially supported by the Russian Foundation for Basic Research (project nos. 18-05-00861 and 18-05-00691). Expedition works (Cruise 37th of the R/V *Professor Logachev*) were financed by the Federal Agency on Nature Management, Ministry of Natural Resources and Ecology of the Russian Federation.

SUPPLEMENTARY MATERIALS

Supplementary materials are available for this article at https://doi.org/10.1134/S0869591120040062 and are accessible for authorized users.

REFERENCES

Aranovich, L.Ya., *Mineral'nye ravnovesiya mnogokomponentnykh tverdykh rastvorov* (Mineral Equilibria of Multicomponent Solid Solutions), Moscow: Nauka, 1991.

Aranovich, L.Ya. and Kosyakova, N.A., Garnet–spinel geothermometer for deep-seated rocks, *Dokl. Akad. Nauk SSSR*, 1980, vol. 254, no. 4, pp. 978–981.

Aranovich, L.Y. and Berman, R.G., Optimized standard state and solution properties of minerals, *Contrib. Mineral. Petrol.,* 1996, vol. 126, nos 1-2, pp. 25–37.

Aranovich, L.Y. and Berman, R.G., A new garnet–orthopyroxene thermometer based on reversed Al_2O_3 solubility in $FeO–Al_2O_3–SiO_2$ orthopyroxene, *Am. Mineral.,* 1997, vol. 82, pp. 345–353.

Asimow, P.D., A model that reconciles major-and trace-element data from abyssal peridotites, *Earth Planet. Sci. Lett.,* 1999, vol. 169, nos. 3–4, pp. 303–319.

Botazzi, P., Ottolini, L., Vannucci, R., and Zanetti, A., An accurate procedure for the quantification of rare earth elements in silicates, *Proceedings of the Ninth International Conference on Secondary Ion Mass Spectrometry-SIMS IX,* Benninghoven, A., Nihei, R., and Shimizu, R., Chichester: John Wiley, 1994.

Brunelli, D., Cipriani, A., Ottolini, L., et al., Mantle peridotites from the Bouvet triple junction region, South Atlantic, *Terra Nova,* 2003, vol. 15, no. 3, pp. 194–203.

Brunelli, D., Seyler, M., Cipriani, A., et al., Discontinuous melt extraction and weak refertilization of mantle peridotites at the Vema lithospheric section (Mid-Atlantic Ridge), *J. Petrol.,* 2006, vol. 47, no. 4, pp. 745–771.

Brunelli, D., Paganelli, E., and Seyler, M., Percolation of enriched melts during incremental open-system melting in the spinel field: a REE approach to abyssal peridotites from the Southwest Indian Ridge, *Geochim. Cosmochim. Acta,* 2014, vol. 127, pp. 190–203.

Dick, H.J., Fisher, R.L., and Bryan, W.B., Mineralogic variability of the uppermost mantle along mid-ocean ridges, *Earth Planet. Sci. Lett.,* 1984, vol. 69, no. 1, pp. 88–106.

Dick, H.J., Abyssal peridotites, very slow spreading ridges and ocean ridge magmatism, *Geol. Soc. London. Spec. Publ.,* 1989, no. 42, pp. 71–105.

D'Errico, ME., Warren, JM., and Godard, M., Evidence for chemically heterogeneous arctic mantle beneath the Gakkel Ridge, *Geochim. Cosmochim. Acta,* 2016, vol. 174, pp. 291–312.

Falus, G., Szabó, C., Kovács, I., et al., Symplectite in spinel lherzolite xenoliths from the Little Hungarian plain, western Hungary: a key for understanding the complex history of the upper mantle of the Pannonian Basin, *Lithos,* 2007, vol. 94, no. 1, pp. 230–247.

Gasparik, T., An internally consistent thermodynamic model for the system cao-mgo-al2o3-SiO_2 derived primarily from phase equilibrium data, *J. Geol.,* 2000, vol. 108, pp. 103–119.

Ghose, I., Cannat, M., and Seyler, M., Transform fault effect on mantle melting in the mark area (Mid-Atlantic Ridge south of the Kane Transform), *Geology,* 1996, vol. 24, no. 12, pp. 1139–1142.

Godard, M., Jousselin, D., and Bodinier, J.L., Relationships between geochemistry and structure beneath a palaeo-spreading centre: a study of the mantle section in the Oman ophiolite, *Earth Planet. Sci. Lett.,* 2000, vol. 180, nos. 1–2, pp. 133–148.

O'Hara, M.J., Richardson, S.W., and Wilson, G., Garnet-peridotite stability and occurrence in crust and mantle, *Contrib. Mineral. Petrol.,* 1971, vol. 32, no. 1, pp. 48–68.

Hellebrand, E., Snow, J.E., Dick, H.J., and Hofmann, A.W., Coupled major and trace elements as indicators of the extent of melting in mid-ocean-ridge peridotites, *Nature,* 2001, vol. 410, no. 6829, pp. 677–681.

Hellebrand, E., Snow, J.E., Hoppe, P., and Hofmann, A.W., Garnet-field melting and late-stage refertilization in residual abyssal peridotites from the Central Indian Ridge, *J. Petrol.,* 2002, vol. 43, no. 12, pp. 2305–2338.

Hofmann, A.W., Chemical differentiation of the earth: the relationship between mantle, continental crust, and oceanic crust, *Earth Planet. Sci. Lett.,* 1988, vol. 90, pp. 297–314.

Irving, A.J. and Frey, F.A., Trace element abundances in megacrysts and their host basalts: constraints on partition coefficients and megacryst genesis, *Geochim. Cosmochim. Acta,* 1984, vol. 48, pp. 1201–1221.

Johnson, K.T.M., Dick, H.J.B., and Shimizu, N., Melting in the oceanic upper mantle: an ion microprobe study of diopsides in abyssal peridotites, *J. Geophys. Res.: Solid Earth,* 1990, vol. 95, no. B3, pp. 2661–2678.

Karson, J.A. and Lawrence, R.M., *Tectonic setting of serpentinite exposures on the western median valley wall of the MARK area in the vicinity of site 920, Proceedings-Ocean Drilling Program Scientific Results. National Science Foundation*, 1997, pp. 5–22.

Kelemen, P.B., Shimizu, N., and Salters, V.J.M., *Focused flow of melt in the upper mantle: extraction ofmorb beneath oceanic spreading ridges*, *Mineral. Mag.,* 1994, vol. A, pp. 466–467.

Komor, S.C., Abyssal peridotite from ODP hole 670a (21°10′ N, 45°02′ W): residues of mantle melting exposed by non-constructive axial divergence, *Proceedings of the Ocean Drilling Program, Scientific Results,* 1990, vol. 106, pp. 85–101.

Kosyakova, N.A., Aranovich, L.Ya., and Podlesskii, K.K., Equilibria of aluminous spinel with orthopyroxene in the system FeO–MgO–Al_2O_3–SiO_2: new experimental data and thermodynamic assessment, *Dokl. Earth Sci.,* 2005, vol. 400, no. 1, pp. 57–61.

Liermann, H.P. and Ganguly, J., Fe^{2+}–Mg fractionantion between orthopyroxene and spinel: experimental calibration in the system FeO–MgO–Al_2O_3–Cr_2O_3–SiO_2, and application, *Contrib. Mineral. Petrol.,* 2003, vol. 145, pp. 217–227.

Malaviarachchi, S.P.K., Makishima, A., and Nakamura, E., Melt–peridotite reactions and fluid metasomatism in the upper mantle, revealed from the geochemistry of peridotite and gabbro from the Horoman peridotite massif, Japan, *J. Petrol.,* 2010, vol. 51, no. 7, pp. 1417–1445.

McCaig, A.M., Cliff, R.A., Escartin, J., et al., Oceanic detachment faults focus very large volumes of Black Smoker fluids, *Geology,* 2007, vol. 35, no. 10, pp. 935–938.

Michael, P.J. and Bonatti, E., Petrology of ultramafic rocks from sites 556, 558 and 560 DSDP, leg 82, *Init. Rep. Deep Sea Drilling Project,* 1985, vol. 82, pp. 523–528.

Morishita, T. and Arai, S., Evolution of spinel–pyroxene symplectite in spinel–lherzolites from the Horoman Complex, Japan, *Contrib. Mineral. Petrol.,* 2003, vol. 144, no. 5, pp. 509–522.

Nicolas, A., *Structures of Ophiolites and Synamics of Oceanic Lithosphere,* Springer Science & Business Media, 2012.

Niu, Y., Langmuir, C.H., and Kinzler, R.J., The origin of abyssal peridotites: a new perspective, *Earth Planet. Sci. Lett.,* 1997, vol. 152, nos. 1–4, pp. 251–265.

Obata, M. and Ozawa, K., Topotaxic relationships between spinel and pyroxene in kelyphite after garnet in mantle-derived peridotites and their implications to reaction mechanism and kinetics, *Mineral. Petrol.,* 2011, vol. 101, nos. 3–4, pp. 217–224.

Odashima, N., Morishita, T., Ozawa, K., et al., Formation and deformation mechanisms of pyroxene–spinel symplectite in an ascending mantle, the Horoman peridotite complex, Japan: an EBSD (electron backscatter diffraction) study, *J. Mineral. Petrol. Sci.,* 2008, vol. 103, no. 1, pp. 1–15.

Pattison, D.R. and Bégin. N.J., Zoning patterns in orthopyroxene and garnet in granulites: implications for geothermometry, *J. Metamorph. Geol.,* 1994, vol. 12, no. 4, pp. 387–410.

Pertsev, A.N., Bortnikov, N.S., Aranovich, L.Ya., et al., Peridotite–melt interaction under transitional conditions between the spinel and plagioclase facies beneath the Mid-Atlantic Ridge: insight from peridotites at 13° N, *Petrology,* 2009, vol. 17, no. 2, pp. 124–137.

Petersen, S., Kuhn, K., Kuhn, T., et al., The geological setting of the ultramafic-hosted Logatchev hydrothermal field (14°45′ N, Mid-Atlantic Ridge) and its influence on massive sulfide formation, *Lithos,* 2009, vol. 112, nos. 1–2, pp. 40–56.

Rampone, E., Romairone, A., and Hofmann, A.W., Contrasting bulk and mineral chemistry in depleted mantle peridotites: evidence for reactive porous flow, *Earth Planet. Sci. Lett.,* 2004, vol. 218, nos. 3–4, pp. 491–506.

Reiners, P.W., Reactive melt transport in the mantle and geochemical signatures of mantle-derived magmas, *J. Petrol.,* 1998, vol. 39, no. 5, pp. 1039–1061.

Searle, R.C. Murton, B.J., et al., Life cycle of oceanic core complexes, *Earth Planet. Sci. Lett.,* 2009, vol. 287, nos. 3–4, pp. 333–344.

Seyler, M., Toplis, M.J., Lorand, J.P., et al., Clinopyroxene microtextures reveal incompletely extracted melts in abyssal peridotites, *Geology,* 2001, vol. 29, no. 2, pp. 155–158.

Seyler, M., Cannat, M., and Mevel, C., Evidence for major-element heterogeneity in the mantle source of abyssal peridotites from the Southwest Indian Ridge (52° to 68° E), *Geochem., Geophys., Geosyst.,* 2003, vol. 4, no. 2. https://doi.org/10.1029/2002GC000305

Seyler, M., Lorand, J.P., Dick, H.J., and Drouin, M., Pervasive melt percolation reactions in ultra-depleted refracto-

ry harzburgites at the Mid-Atlantic Ridge, 15°20′ N: ODP hole 1274a, *Contrib. Mineral. Petrol.,* 2007, vol. 153, no. 3, pp. 303–319.

Shannon, R.D., Revised effective ionic radii and systematic studies of interatomic distances in halides and chacogenides, *Acta Crystallogr. Sect. A,* 1976, vol. 32, pp. 751–767.

Shimizu, N. and Hart, S.R., Application of the ion microprobe to geochemistry and cosmochemistry, *Annu. Rev. Earth Planet. Sci.,* 1982, vol. 10, pp. 483–526.

Shimizu, Y., Arai, S., Morishita, T., and Ishida, Y., Origin and significance of spinel–pyroxene symplectite in lherzolite xenoliths from tallante, SE Spain, *Mineral. Petrol.,* 2008, vol. 94, nos. 1–2, pp. 27–43.

Smith, D.K., Escartin, J., Schouten, H., and Cann, J.R., Fault rotation and core complex formation: significant processes in seafloor formation at slow-spreading mid-ocean ridges (Mid-Atlantic Ridge, 13°–15° N), *Geochem., Geophys., Geosyst.,* 2008, vol. 9, no. 3.
https://doi.org/10.1029/2007GC001699

Sobolev, A.V., Melt inclusions in minerals as a source of principal petrological information, *Petrology,* 1996, vol. 4, pp. 228–239.

Stephens, C.J., Heterogeneity of oceanic peridotite from the Western Canyon wall at mark: results from site 920, *Proceedings of the Ocean Drilling Program, Scientific Results,* 1997, vol. 153, pp. 285–303.

Suhr, G., Melt migration under oceanic ridges: inferences from reactive transport modelling of upper mantle hosted dunites, *J. Petrol.,* 1999, vol. 40, no. 4, pp. 575–599.

Suhr, G., Kelemen, P., and Paulick, H., Microstructures in hole 1274a peridotites, ODP leg 209, Mid-Atlantic Ridge: tracking the fate of melts percolating in peridotite as the lithosphere is intercepted, *Geochem., Geophys., Geosyst.,* 2008, vol. 9, no. 3.
https://doi.org/10.1029/2007gc001726

Sun, S.-S. and McConough, W.F., *Chemical and isotopic systematics of oceanic basalts: implications for mantle composition and processes, Magmatism in the Ocean Basins*, Saunders, A.D. and Norry, V.J., Eds., *Geol. Soc. Spec. Publ.,* 1989, vol. 42, pp. 313–345.

Walter, M.J., Melt extraction and compositional variability in mantle lithosphere, *Treatise on Geochemistry,* 2003, vol. 2, pp. 363–393.

Wang, J., Zhou, H., Salters, V., et al., Mantle melting variation and refertilization beneath the Dragon Bone amagmatic segment (53° E SWIR): major and trace element compositions of peridotites at ridge flanks, *Lithos*, 2019, vol. 324, pp. 325–339.

Wood, B.J. and Blundy, J.D., A predictive model for rare earth element partitioning between clinopyroxene and anhydrous silicate melt, *Contrib. Mineral. Petrol.,* 1997, vol. 129, pp. 166–181.

Yoder, H.S., *Generation of Basaltic Magma,* Washington, DC: National Academy of Sciences, 1976.

Translated by M. Bogina